Journal of
Computational and Theoretical Nanoscience
Vol. 5, 449–463, 2008

REVIEW

Theoretical Modeling on Mechanical-Electrical Coupling of Carbon Nanotubes

Jun-Qiang Lu[1] and Hanqing Jiang[2,*]

[1] Center for Nanophase Materials Sciences, Oak Ridge National Laboratory, Oak Ridge, Tennessee 37831, USA
[2] Department of Mechanical and Aerospace Engineering, Arizona State University, Tempe, Arizona 85287, USA

Carbon nanotubes have been studied extensively due to their unique properties, ranging from electronic, mechanical, optical, to thermal properties. The coupling between the electronic and mechanical properties of carbon nanotubes has emerged as a new field, which raises both interesting fundamental problems and fantastic application potentials. In this article, we will review our recent work on the theoretical modeling on mechanical-electrical coupling of carbon nanotubes subject to various loading conditions, including tension/compression, torsion, and squashing. Some related work by other groups will be also mentioned.

Keywords: Carbon Nanotubes, Mechanical/Electronic Coupling, Metal-Semiconductor Transition.

CONTENTS

1. INTRODUCTION

Since the first discovery of carbon nanotubes (CNTs),[1] they have been attracting significant attention due to their superior advantages, including mechanical properties, low mass density, and especially electrical properties. The fascinating electrical properties of carbon nanotubes result from their high-symmetrical crystal structures. A single wall CNT (SWCNT) can be imaginarily formed by cutting a honeycomb lattice of graphite sheet followed by rolling it up in certain direction on a cylindrical surface. The cutting and rolling direction of CNTs can be expressed by the standard notation of one pair of integers (n,m), which is called the chirality of the CNT. Several special cases are: $(n,0)$ and (n,n) are called zigzag and armchair CNTs, respectively, while the general case $n > |m| > 0$ is called a chiral CNT. For a given (n,m) CNT, if $n-m$ is a multiple of 3, then the CNT is metallic; otherwise the CNT is a semiconductor. More interesting, the electrical properties of carbon nanotubes can be altered by mechanical deformation in experiments. Those mechanical deformations can be divided into (1) bending; (2) stretching; (3) squashing (radial deformation); and (4) torsion.

For bending deformation, Tombler et al.[2] investigated the electrical conductance change for a single wall CNT due to mechanical bending. The CNT was bent mechanically by the tip of an atomic force microscope (AFM) and the electrical conductance change was measured simultaneously upon mechanical deformation. It was found that the electrical conductance may change by two orders of magnitude upon mechanical deformation. Minot et al.[3] conducted the similar experiments and found the same trend that the bending strain can open a band gap in a metallic CNT and modify the band gap in a semiconducting CNT. Semet et al.[4] studied the conductance change of multi-wall CNTs due to bending and observed that the nonlinear change of conductance is reversible.

For stretching, Cao et al.[5] designed a MEMS-based test stage to measure the electric-mechanical properties for CNTs under uniform tensile stretching. They found that the armchair CNTs exhibit least sensitivity to tensile strain characterized by very small band gap opening; while other metallic CNTs ($n-m$ is a multiple of 3 but not 0) are sensitive to the tensile strain by large band gap opening. Those observations qualitatively agree with other theoretical studies.[6–10]

*Author to whom correspondence should be addressed.

1546-1955/2008/5/449/015 doi:10.1166/jctn.2008.003

REVIEW

For squashing or radial deformation, Gómez-Navarro et al.[11, 12] used AFM tip to generate radial deformation. In their experiments, a sample of random distributed single wall CNTs were deposited on an insulating substrate. Once the position along the length of the CNT was selected, the AFM tip was placed on top of this position and the sample started to move towards the AFM tip. For each step of the movement, a ramp of voltage to the AFM tip was applied and the loading force, the electrical current, and the differential conductance were simultaneously measured. They found that the band gap was opened before the tube was fully collapsed and that open-close cycles of the band gap were present during the radial deformation.

In a recent publication, Cohen-Karni et al.[13] measured the conductance change due to torsional deformation. A MEMS-based torsion experimental stage was designed, where a suspended multiwalled CNT is mechanically and electrically connected to a pair of electrodes and a small pedal in the middle of CNT. The multiwalled CNT was twisted by pressing against the pedal with an AFM tip, and the conductance across the multiwalled CNT was simultaneously measured through the two electrodes. By pressing the pedal with the AFM tip, the chirality of CNT will change continuously and periodically and so that the torsional deformation will induce conductance oscillations, which was also observed in the experiments.

All the above mentioned experiments indicate that the mechanical deformation can significantly affect the electrical properties, which makes CNTs excellent candidates for nano-devices such as nanoscale field-effect transistors, nanoscale sensors and nano-electro-mechanical systems (NEMS).[14, 15]

In this review, we will review some recently progress of the theoretical modeling on mechanical-electrical coupling of CNTs subject to various loading conditions, including tension/compression, torsion, and squashing. For uniform deformation as tension/compression and torsion, the periodic crystal structure will remain, while the squashing deformation will alter the periodic crystal structure since the deformation is non-uniform. In the following, we will summarize the theoretical modeling efforts according to uniform and non-uniform deformation.

2. UNIFORM DEFORMATION: TENSION/COMPRESSION AND TORSION

The first step on mechanical-electrical coupling analysis is to determine the atom positions upon deformation, which can be done by many means, such as molecular mechanics (MM), molecular dynamics (MD), tight-binding simulations (TB), and *ab initio*, etc. MM, MD determine the atom positions upon mechanical deformation by following each atom and therefore they are computational expensive. Given the nature of uniform deformation, a representative element can be selected and the entire deformation of the CNT can be studied in the continuum point of view.

The nanoscale continuum theory for CNT was developed by Zhang, Jiang and co-workers,[16–19] based on the interatomic potential for carbon.[20] Unlike MD simulations that keep tracking of every atom, the proposed nanoscale continuum theory represents the collective behavior of a few atoms based on the modified Cauchy-Born rule.[21] The Cauchy-Born rule equates the strain energy on the continuum level to the bond potential energy on the atomic

Jun-Qiang Lu is a Postdoctoral Research Associate at Center for Nanophase Materials Sciences, Oak Ridge National Laboratory, U.S. Department of Energy. He received his B.S. degree from Department of Physics, Tsinghua University, China in 1998, and Ph.D. degree from Center for Advanced Study, Tsinghua University, China in 2003. He was a Postdoctoral Research Associate at Department of Mechanical and Industrial Engineering, University of Illinois at Urbana-Champaign from 2004 to 2005. His research interests are in theoretical condensed matter physics and computational material science, including: developing electronic transport and electronic structure programs from both tight-binding and first principle levels; electromechanical properties of carbon nanotubes and semiconductor nanostructures; polyphenylene-based molecular electronics and device designs; and spintronics. He received the National Excellent Doctoral Dissertation Award from the Ministry of Education, China in 2005.

Dr. Hanqing Jiang received Ph.D. from Tsinghua University in 2001. Before he joined the faculty in the Department of Mechanical and Aerospace Engineering at Arizona State University as an assistant professor in 2006, he was a Research Scientist at the University of Illinois at Urbana-Champaign. His current research interest is the multi-scale materials modeling and simulation with emphasis on multifield interactions, including atomistic-based continuum theory, atomic-scale finite element method, nanocomposites, electronic-mechanical coupling of carbon nanotubes, and stretchable electronics as well as biomechanics. He has published 29 peer-reviewed journal papers. Many of his papers are among the top cited papers in mechanics and/or mechanical engineering communities.

level and also states that all atoms (on the atomic level) are subject to a homogeneous deformation and move according to a single mapping from the undeformed to the deformed configurations. In other words, the Cauchy-Born rule enforces a simple deformation pattern for all atoms in the system. For a centrosymmetric atomic structure with pair of bonds in the opposite directions around each atom, the forces due to deformation are in the opposite direction with same magnitude and can be cancelled so that the equilibrium of atoms can be achieved by the Cauchy-Born rule. If the atomic structure is not centrosymmetric, such as CNTs with hexagonal lattice, the forces do not appear in opposite direction and cannot be cancelled; therefore Cauchy-Born rule cannot ensure the equilibrium for CNTs. Despite that the simple mapping from undeformed to deformed configurations cannot ensure the equilibrium, some researchers[7,8] still used it to determine the atom position and the induced electrical properties changes, which will lead to significant difference as to be shown.

In order to ensure the equilibrium for non-centrosymmetric structure, the Cauchy-Born rule must be modified. Zhang, Jiang and co-workers[16–19] have modified the Cauchy-Born rule to ensure the equilibrium for non-centrosymmetric atomic structures. A hexagonal lattice structure of CNT can be decomposed into two triangular sub-lattices, as shown in Figure 1. Each sub-lattice has the centrosymmetric structure and therefore follows the Cauchy-Born rule. However, the two sub-lattices may undergo a relative shift $\boldsymbol{\zeta}$ to release the energy due to the assumption of single mapping. This shift $\boldsymbol{\zeta}$ represents an internal degree of freedom for the hexagonal lattice structure and remains to be determined by enforcing the equilibrium of atoms. The shift vector $\boldsymbol{\zeta}$ is determined by minimizing the strain energy density W with respect to $\boldsymbol{\zeta}$, i.e.,

$$\frac{\partial W}{\partial \boldsymbol{\zeta}} = 0 \tag{1}$$

which is equivalent to the equilibrium of each atom in the hexagonal lattice structure possessing no centrosymmetry. Then the bond length in the same sub-lattice (e.g., distance from atoms B and C in Fig. 1) is given by

$$r_{\mathrm{BC}} = \sqrt{\boldsymbol{r}_{\mathrm{BC}}^{(0)} \cdot (\boldsymbol{I} + 2\boldsymbol{E}) \cdot \boldsymbol{r}_{\mathrm{BC}}^{(0)}} \tag{2}$$

and the bond length between two atoms from different sub-lattices (e.g., atoms A and B) after deformation is given by

$$r_{\mathrm{AB}} = \sqrt{\boldsymbol{\zeta} \cdot \boldsymbol{\zeta} + 2\boldsymbol{\zeta} \cdot \boldsymbol{F} \cdot \boldsymbol{r}_{\mathrm{AB}}^{(0)} + \boldsymbol{r}_{\mathrm{AB}}^{(0)} \cdot (\boldsymbol{I} + 2\boldsymbol{E}) \cdot \boldsymbol{r}_{\mathrm{AB}}^{(0)}} \tag{3}$$

where $\boldsymbol{F} = \partial \boldsymbol{x} / \partial \boldsymbol{X}$ is the deformation gradient and characterizes the deformation on the continuum level; $\boldsymbol{x}$ and $\boldsymbol{X}$ denote the positions of a material point in the deformed and undeformed configurations, respectively; $\boldsymbol{E} = (1/2)(\boldsymbol{F}^T \cdot \boldsymbol{F} - \boldsymbol{I})$ is the Green strain and $\boldsymbol{F}^T$ and $\boldsymbol{I}$ are the transpose of $\boldsymbol{F}$ and the second order identity tensor; $\boldsymbol{r}_{ij}^{(0)}$ is the vector from atoms i to j before the deformation.

The atom positions then can be determined for specific loading. For tension/compression, the strain (E_{ZZ}) in the axial direction is given and the strain in the circumferential direction ($E_{\theta\theta}$) and the shift vector $\boldsymbol{\zeta}$ can be obtained by using vanishing circumferential stress condition and the energy minimization with respect to shift vector $\boldsymbol{\zeta}$. For torsion, once the torsional angle is given, the similar method can be conducted to obtain the atom position after deformation. For example, a bond parallel to the tension direction will change from 0.146 nm before deformation to 0.159 nm after deformation for 10% tensile strain. The results of the atom positions using the nanoscale continuum theory is as accurate as molecular mechanics, as shown in Liu et al.[22] Compared with the Cauchy-Born rule where all atoms follow the same deformation pattern, the same bond becomes 0.161 nm long for the same 10% tensile strain. Although the difference in bond length is very small, as shown in the following, the difference in electrical properties is significant.

Once the atom positions are determined, the tight-binding method will be used to study the electrical properties of the deformed CNT under tension/compression, torsion, and combined tension and torsion. Since these deformations are uniform, i.e., the deformed CNT still possess translational symmetry, the k-space tight-binding method can be used, which significantly reduces the computational efforts by using the translational symmetry. The k-space tight-binding method has been used to study the electrical property of undeformed CNTs.[23] The unit cell used in k-space tight-binding method is shown in Figure 2, where each unit cell has two inequivalent atoms (A and B),

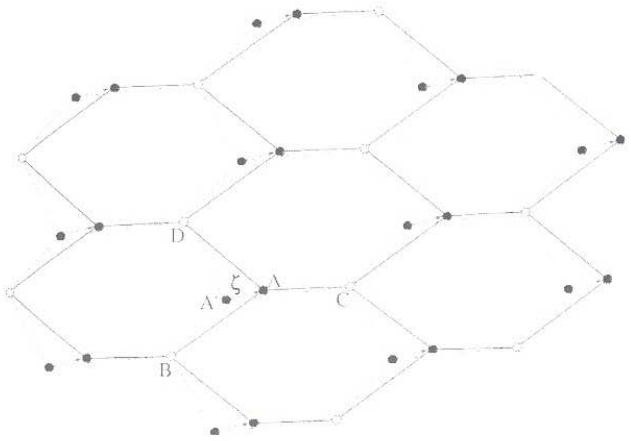

Fig. 1. The decomposition of a hexagonal lattice of carbon nanotube, imaginarily formed from a planar sheet of graphite, to two triangular sub-lattices. There is a shift vector $\boldsymbol{\zeta}$ between two sub-lattices to ensure the equilibrium of atoms. The solid and dashed lines denote the lattice structures with and without the shift vector $\boldsymbol{\zeta}$, respectively. Reprinted with permission from [22], B. Liu et al., *J. Mech. Phys. Solids* 52, 1 (**2004**). © 2004, Elsevier.

REVIEW

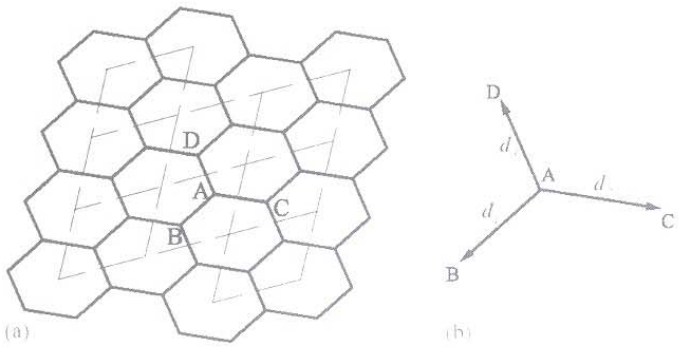

Fig. 2. The representative atom A and its three nearest neighbor atoms B, C and D for the k-space tight-binding calculation. (a) Unit cells and (b) atom positions. Reprinted with permission from [22], B. Liu et al., *J. Mech. Phys. Solids* 52, 1 (**2004**). © (2004), Elsevier.

and $\boldsymbol{d}_1$, $\boldsymbol{d}_2$, $\boldsymbol{d}_3$ are used to characterize the deformation for each unit cell. Remarkably, those three vectors depend on deformation gradient $\boldsymbol{F}$ and shift vector $\boldsymbol{\zeta}$. The tight-binding Hamiltonian is an 8×8 matrix since there are two atoms in each unit cell and is given by

$$\boldsymbol{H}(k) = \begin{bmatrix} \varepsilon_s & 0 & 0 & 0 & H^{ss} & H^{sx} & H^{sy} & H^{sz} \\ 0 & \varepsilon_p & 0 & 0 & -H^{sx} & H^{xx} & H^{xy} & H^{xz} \\ 0 & 0 & \varepsilon_p & 0 & -H^{sy} & H^{xy} & H^{yy} & H^{zy} \\ 0 & 0 & 0 & \varepsilon_p & -H^{sz} & H^{xz} & H^{yz} & H^{zz} \\ H^{ss*} & -H^{sx*} & -H^{sy*} & -H^{sz*} & \varepsilon_s & 0 & 0 & 0 \\ H^{sx*} & H^{xx*} & H^{xy*} & H^{xz*} & 0 & \varepsilon_p & 0 & 0 \\ H^{sy*} & H^{yx*} & H^{yy*} & H^{yz*} & 0 & 0 & \varepsilon_p & 0 \\ H^{sz*} & H^{zx*} & H^{zy*} & H^{zz*} & 0 & 0 & 0 & \varepsilon_p \end{bmatrix} \quad (4)$$

where only the near-neighbor interaction is considered; $\boldsymbol{k}$ is the wave vector; ε_s and ε_p are the orbital energies of s and p orbitals, respectively; $H^{\alpha\beta}$ terms represent interactions between α orbital and β orbital of neighboring atoms, where α and β can be s and p orbitals; $H^{\alpha\beta*}$ are the complex conjugate of $H^{\alpha\beta}$. $H^{\alpha\beta}$ terms depend on wave vector $\boldsymbol{k}$ and the specific expression was given by Xu et al.[24]

The wave vector $\boldsymbol{k}$ in the Hamiltonian matrix (4) is quantized because of the periodic boundary condition in the circumferential direction for a CNT, and is given by

$$\boldsymbol{k} = k_t \frac{\boldsymbol{K}}{|\boldsymbol{K}_2|} + \mu \boldsymbol{K}_1 \left(\mu = 0, \ldots, N-1, \text{ and } -\frac{\pi}{|\boldsymbol{T}|} < k_t < \frac{\pi}{|\boldsymbol{T}|} \right) \quad (5)$$

where k_t is the translational (axial) component of the wave vector $\boldsymbol{k}$; N is the number of the hexagons in the area of $|\boldsymbol{C}_h \times \boldsymbol{h}|$, $\boldsymbol{K}_1 = (2\pi \boldsymbol{C}_h)/|\boldsymbol{C}_h|^2$ and $\boldsymbol{K}_2 = (2\pi \boldsymbol{T})/|\boldsymbol{T}|^2$ are the reciprocal lattice vectors, $\boldsymbol{C}_h$ and $\boldsymbol{T}$ are the chiral and translational vectors of the deformed CNT.

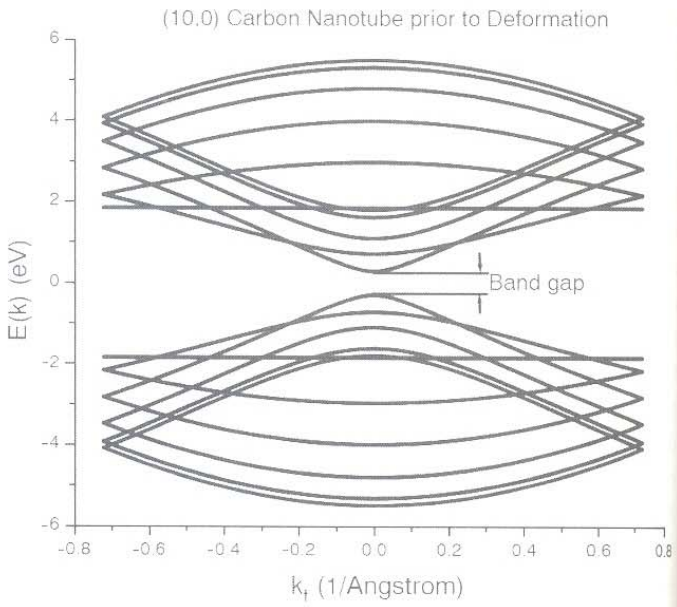

Fig. 3. The energy dispersion relations for a zigzag (10,0) carbon nanotube prior to deformation. Reprinted with permission from [22], B. Liu et al., *J. Mech. Phys. Solids* 52, 1 (**2004**). © (2004), Elsevier.

For each wave vector $\boldsymbol{k}$ in (5), the energy eigenstates can be solved by diagonalizing the Hamiltonian matrix in (5). Once the energy eigenstates are determined for all wave vectors, the energy dispersion relations for σ and π bands are obtained, which give the band gap of the deformed CNT. Figure 3 shows an example of the energy dispersion relations for a zigzag (10,0) CNT prior to deformation. The energy states are shown versus the axial component k_t of the wave vector $\boldsymbol{k}$ for all quantized μ in (5). Here the band gap is an indicator of whether the CNT is electrically conducting: zero band gap corresponds to electrically conducting materials, while a non-vanishing, finite band gap generally corresponds to semi-conducting materials.

As mentioned before, the small difference in atom position between the original and the modified Cauchy-Born rule will induce significant difference in electrical properties. Figure 4 shows the band gap versus the engineering tensile strain ε ($=F_{ZZ}-1$) for a (9,0) CNT under tension with and without shift vector $\boldsymbol{\zeta}$. It is clearly shown that the band gap exhibits differently although the trend is the same. For example, when the strain is 10%, the band gap based on the original Cauchy-Born rule that has no shift vector is significantly overestimated by a factor of 6.[7] Therefore, the shift vector $\boldsymbol{\zeta}$ plays an important role in electrical properties.

Figure 5 shows the band gap versus the engineering strain ε for (5,5), (9,0), (9,6), (10,0), and (6,4) CNTs to investigate how the tensile deformation affects the electrical properties. The band gap for the armchair (5,5) CNT does not change with tensile strain and keeps zero. In fact this conclusion has been confirmed by other (n,n) armchair CNTs, i.e., they remain conducting under tension. For the conducting zigzag (9,0) and chiral (9,6) CNTs the band gap generally increases with tensile strain, which

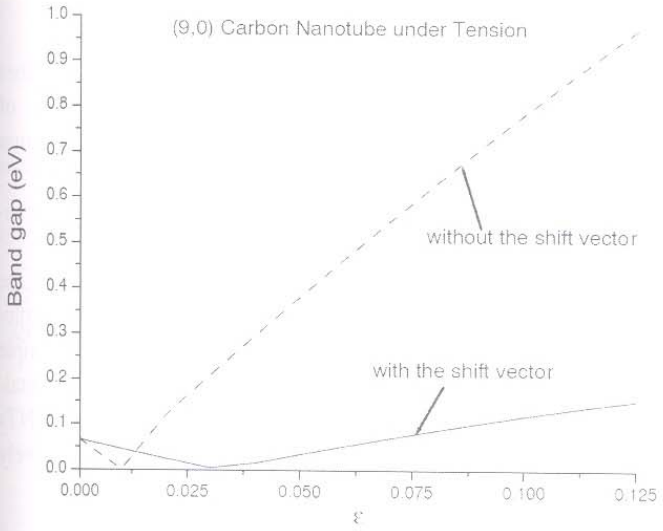

Fig. 4. The band gap versus the tensile strain ε for a (9,0) carbon nanotube under tension. The results are shown for calculations with and without the shift vector ζ. Reprinted with permission from [22], B. Liu et al., *J. Mech. Phys. Solids* 52, 1 **(2004)**. © (2004), Elsevier.

suggests that the conducting CNTs may become semi-conducting upon tensile deformation. However, the band gap for the semi-conducting zigzag (10,0) and chiral (6,4) CNTs, remains large despite that it displays some variation upon deformation. This suggests that the tensile deformation cannot alter a semi-conducting CNT to conducting CNT. The tensile deformation induced electrical properties change, especially the change from a conducting CNT to semi-conducting, is both theoretically and practically important. In theoretical point of view, the widely accepted criterion ($n - m$ is multiply of 3) for conducting CNT does not hold anymore once upon the tensile deformation. In practical application, this conducting/semi-conducting transition can be applied to design mechanical-electrical sensors.

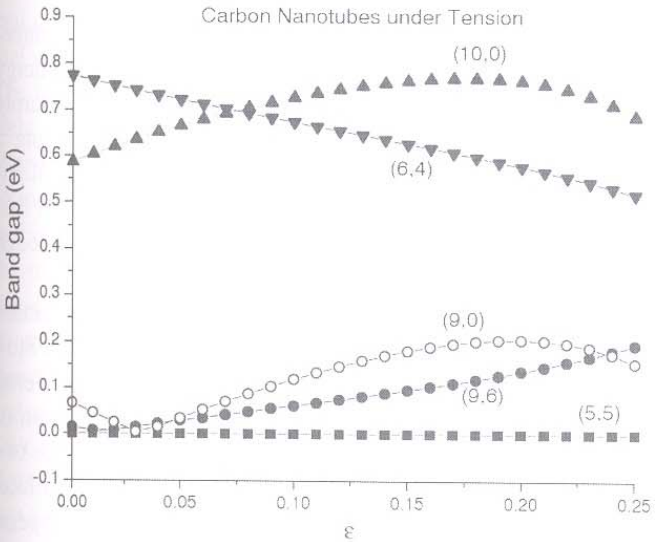

Fig. 5. The band gap versus the tensile strain ε accounting for the shift vector for various carbon nanotubes under tension. Reprinted with permission from [22], B. Liu et al., *J. Mech. Phys. Solids* 52, 1 **(2004)**. © (2004), Elsevier.

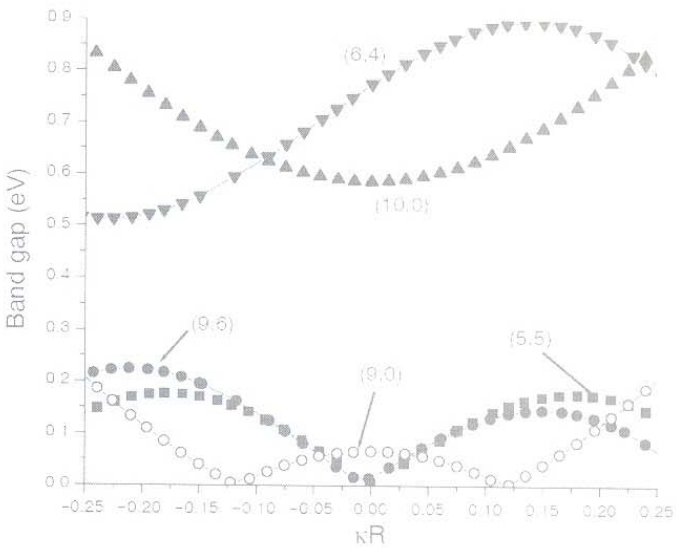

Fig. 6. The band gap versus the normalized twist κR accounting for the shift vector for various carbon nanotubes (CNT), where κ is the twist (rotation per unit length) and R is the radius of the CNT. The results are shown for calculations with and without the shift vector. Reprinted with permission from [22], B. Liu et al., *J. Mech. Phys. Solids* 52, 1 **(2004)**. © 2004, Elsevier.

The similar studies were also conducted for torsion. Figure 6 shows the band gap versus the normalized twist, κR, for (5,5), (9,0), (9,6), (10,0), and (6,4) CNTs under torsion, where R is the CNT radius prior to deformation. Since the torsion is symmetric, i.e., a pair of opposite angle of twist κ means that CNT is twisted in opposite direction with same amount of torsional angle, the band gap for symmetric CNTs (i.e., armchair and zigzag CNTs) is also symmetric; while the curve is unsymmetric for chiral CNTs. Contrary to tension, the band gap of armchair (5,5) CNT is not zero anymore once torsion is imposed; it varies from zero to a finite amount. This trend is also observed in other metallic CNTs, including (9,0) and (9,6) CNTs, where band gap varies upon torsional deformation. Similar to tension, the band gap for semi-conducting CNTs keeps finite no matter the torsional strain. The same transition from metallic to semi-conducting CNTs for tension and torsion make metallic CNTs unique candidates for mechanical-electrical sensors. For chiral CNTs that originally have finite band gap, the torsional deformation does not qualitatively change the electrical properties, i.e., semi-conducting property remains before and after torsional deformation.

The combined tension/torsion deformation was also imposed to CNTs. Figure 7 shows the distribution of band gap versus the tensile (engineering) strain ε and normalized twist κR for (5,5) CNT. Only $\kappa R \geq 0$ is shown due to symmetry. It is observed that the band gap is non-zero almost over the entire domain; only around very isolated curves does the band gap vanish. This is clearly observed from the contour plot of band gap in Figure 7(b). The isolated curves for vanishing band gap are marked by the white dashed lines. Therefore, even though these three

REVIEW

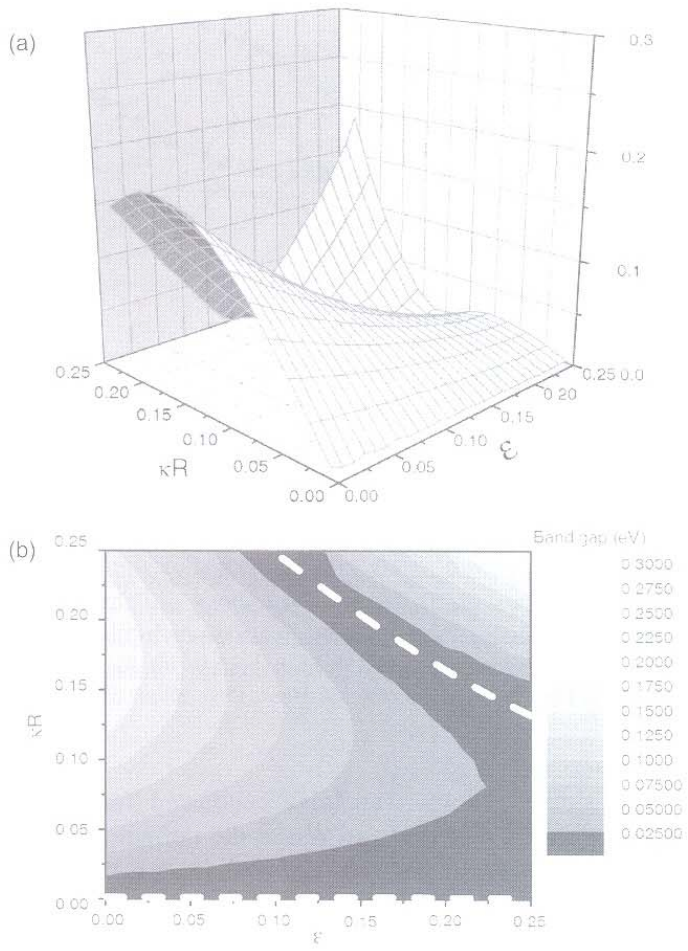

Fig. 7. The band gap versus the tensile strain ε and normalized twist κR for (5,5) carbon nanotubes (CNT) under combined tension/torsion. (a) (5,5) CNT (b) contour plot. Reprinted with permission from [22], B. Liu et al., *J. Mech. Phys. Solids* 52, 1 **(2004)**, © 2004, Elsevier.

CNTs are considered as conducting by the simple criterion ($n-m$ is the multiply of 3), their band gap will most likely become finite and the conducting CNTs will become semi-conducting once the deformation is imposed.

3. NON-UNIFORM DEFORMATION: SQUASHING

Electronic properties of nanotubes can be changed dramatically by squashing. As mentioned earlier, metal-semiconductor, semiconductor-metal and metal-semiconductor-metal transitions by squashing nanotubes have been experimentally demonstrated.[5,6] In these experiments, squashing was preformed by an AFM tip. The squashing of nanotube under the AFM tip is localized and the deformation far away from the tip decays and the strain is small. Extensive theoretical studies[21–28] have been carried out on the simple model of radial deformation with infinite length, which described a comprehensive picture of the metal-semiconductor, semiconductor-metal and metal-semiconductor-metal transitions. Studies[25] of the finite size effect of the squashing are particular important for NEMS design.

3.1. Radial Deformation

The electronic property transition of carbon nanotubes under radial deformation varies for different type of nanotubes. For example, metal-semiconductor transition occurs when armchair SWCNTs are squashed,[21, 22, 26–28] and metal-semiconductor and semiconductor-metal transitions happen when zigzag SWCNTs are squashed.[21–27] If deformation is applied at different locations of the SWCNT, it will produce series of semiconductor structures along the SWCNT axis, which opens a very simple idea to build nanoscale circuits. Due to this reason, metal-semiconductor transition (MST) in squashing SWCNTs are particular important and have been comprehensively studied.[21–28]

3.1.1. MST in Squashing Armchair SWCNTs

MST in squashing (or, radial deformation) armchair SWCNTs has been studied extensively.[26–30] Park et al.[26] investigated the mirror symmetry breaking related to the MST. Lammert et al.[27] pointed out the role of the interaction between carbon bilayer-structure in squashed SWCNTs. We[30] studied the combined effect of mirror symmetry breaking and bond formation between the flattened faces of the squashed SWCNTs, and proposed a general guide line to achieve MST in an armchair SWCNTs by making the two original equivalent sublattices physically distinguishable. This guide line may also be applicable beyond mechanical deformation, such as chemical absorption.

The typical conductance curve of a perfect armchair (8,8) SWCNT is shown in Figure 8(a). The conductance near the Fermi energy is $2G_0$, indicating that there are two conducting channels. There are two different means to squash an armchair SWCNT: one by breaking the mirror symmetry about the y-axis (Figs. 8(b and c)) and the other by preserving the mirror symmetry (Fig. 8(e)).

When the SWCNT is squashed without mirror symmetry, its conductance remains at $2G_0$ near the Fermi energy with an elliptical shape (Fig. 8(b)), but drops sharply to zero with a dumbbell shape (Fig. 8(c)), indicating MST has be achieved. The difference between an elliptical SWCNT and a dumbbell SWCNT is that the two flattened faces in a dumbbell SWCNT become close enough to interact with each other.

The relationship between the MST and the interaction between the two flattened faces is showed in Figure 8(d). Figure 8(d) plots the conductance gap near the Fermi energy and the interaction distance $d_{AA'}$ as a function of the tip separation d_y. $d_{AA'}$ is the distance between the two closest atoms, A in the upper face and A′ in the lower face as shown in Figure 8(b). The conductance gap appears when $d_{AA'} < 2.60$ Å, indicating that the gap is opened after the atom A starts to interact with the atom A′.

However, the interaction alone is not sufficient to induce a MST. When the SWCNT is squashed with the

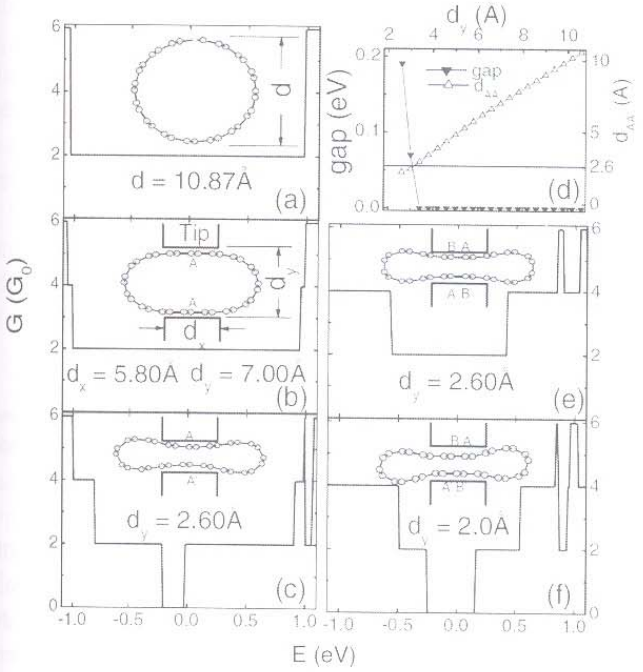

Fig. 8. (a–c), (e, f) Conductances of various SWCNT structures, which are shown as the insets. E is the energy of conducting electrons. The Fermi energy of ideal armchair (8,8) SWCNT is taken as zero. (d) The conductance gap and $d_{AA'}$ as a function of the tip distance d_y. Reprinted with permission from [30], J. Q. Lu et al., *Phys. Rev. Lett.* 90, 156601 (**2003**). © 2003, The American Physical Society.

mirror symmetry preserved, as shown in Figure 8(e), the conductance remains at $2G_0$ near the Fermi energy, even when the distance between the two flattened faces is less than 2.60 Å. Thus, a MST has to be driven by the combined effect of the mirror symmetry breaking and interaction between the two flattened faces.

The combined effect of the mirror symmetry breaking and the interaction between the flattened faces in a squashed armchair SWCNT can be viewed as a more general condition for driving the MST: to make the two original equivalent sublattices in the SWCNT distinguishable. The nanotubes, similar to graphene sheet, have two equivalent sublattices, which labeled as A and B sublattices. When a SWCNT is squashed along the axis through two atoms from the same A-sublattice (or B-sublattice), as in Figures 8(b and c), the squashed SWCNT will break the mirror symmetry about the axis. When the two flattened faces are close enough, A-atoms will interact with A-atoms. If the squashing is performed along the axis through two atoms from different sublattices (one from A and the other from B), as in Figure 8(e), the squashed SWCNT will maintain the mirror symmetry. When the two flattened faces are close enough, A(B)-atoms interact with B(A)-atoms. In the following, the first case will be referred as the AA′ structure (Fig. 8(c)) and the second as the AB′ structure (Fig. 8(e)).

The MST in squashing armchair SWCNT can be understood by an extended simple ppπ model which includes the interaction between the two flattened faces. The interaction can be expressed by a perturbation Hamiltonian[31]

$$H'(k) = \begin{pmatrix} \delta_{\pi\pi}(k) & \delta_{\pi\pi^*}(k) \\ \delta_{\pi^*\pi}(k) & \delta_{\pi^*\pi^*}(k) \end{pmatrix} \tag{6}$$

The diagonal terms $\delta_{\pi\pi}(k)$ and $\delta_{\pi^*\pi^*}(k)$ shift the π and π^* bands, and the band crossing point. The off-diagonal terms $\delta_{\pi^*\pi}(k)$ and $\delta_{\pi\pi^*}(k)$ will open up an energy gap. If a mirror symmetry exists, such as AB′ structure, then $M(\pi) = \pi$; $M(H') = H'$; $M(\pi^*) = -\pi^*$, where M is the mirror operator. Consequently, $\delta_{\pi\pi^*} = M(\delta_{\pi\pi^*}) = M(\langle\pi|H'|\pi^*\rangle) = -\langle\pi|H'|\pi^*\rangle = -\delta_{\pi\pi^*}$, which gives $\delta_{\pi\pi^*} = 0$. That means the off-diagonal terms are always zero and no band gap opening.

Figure 9(d) schematically represents the interactions between the two states π and π^* for the two structures AA′ and AB′. As shown by the figure, the off-diagonal term of the AA′ structure $\delta_{\pi\pi^*}$ consists of two σ bonds as $\delta_{\pi\pi^*} = \langle p|H'|p\rangle + \langle p|H'|p\rangle \neq 0$, where $|p\rangle$ is the $2p_y$ orbital of carbon atom. The off-diagonal term

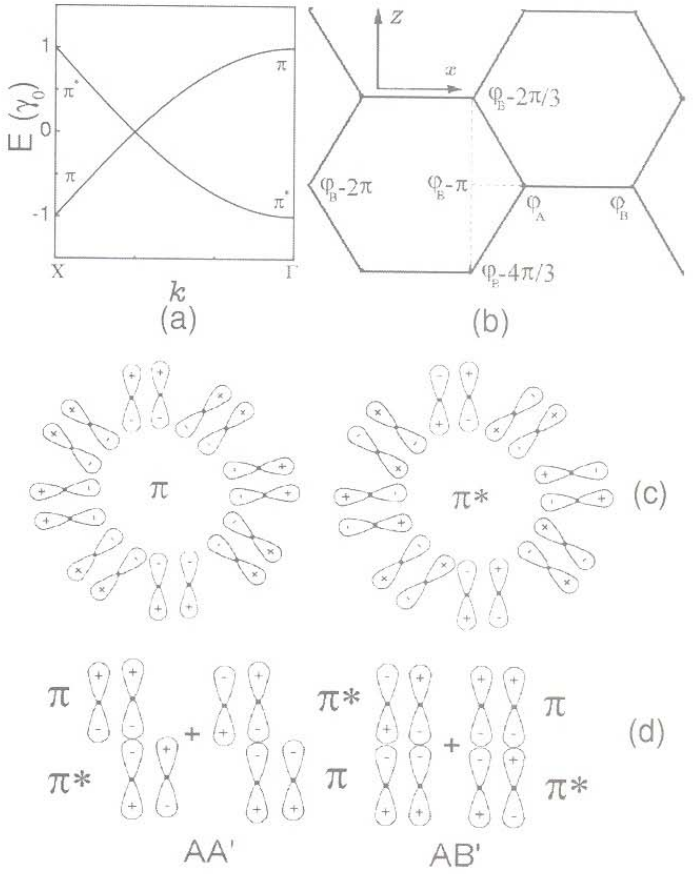

Fig. 9. (a) The energy dispersion relations near the Fermi energy of an ideal armchair (8,8) SWCNT with a ppπ model. (b) The phase correlations at the Fermi vector k_f between the three equivalent atomic positions B which are the nearest neighborhoods of the atomic positions A. (c) A schematic representation of the state π and π^* within the cross section of an ideal armchair (8,8) SWCNT. (d) Configurations of the new interaction introduced between the π state and π^* state for structures AA′ and AB′. Reprinted with permission from [30], J. Q. Lu et al., *Phys. Rev. Lett.* 90, 156601 (**2003**). © 2003, The American Physical Society.

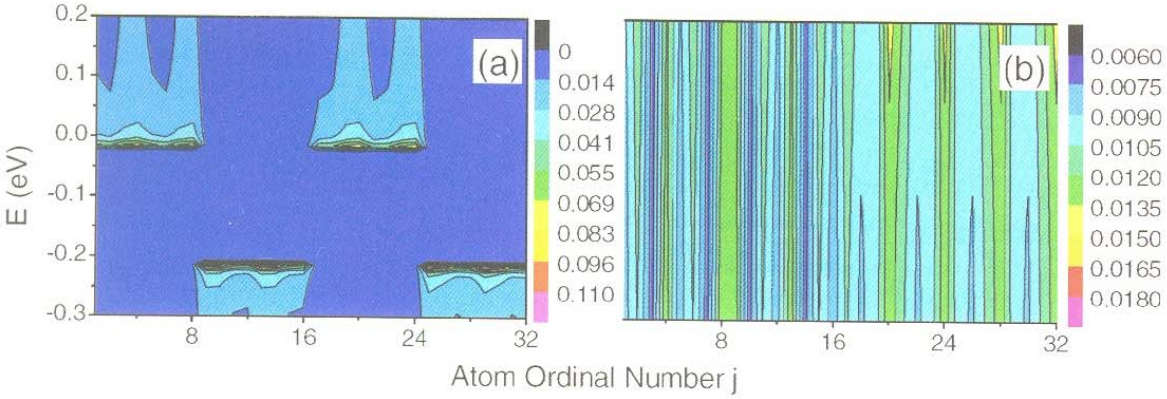

Fig. 10. The LDOS (unit: eV^{-1}) distributions near the Fermi energy over two atomic layers of the squashed (8,8) armchair SWCNT for AA′ (a) and AB′ (b) structures. The atoms in B (A) sublattice are labled 1 (9) through 8 (16) for the first atomic layer and 17 (25) through 24 (32) for the second atomic layer. Reprinted with permission from [30], J. Q. Lu et al., *Phys. Rev. Lett.* 90, 156601 **(2003)**. © 2003, The American Physical Society.

of the AB′ structure consists of four σ bonds, which cancel out as $\delta_{\pi\pi^*} = (-\langle p|H'|p\rangle + \langle p|H'|p\rangle + \langle p|H'|p\rangle - \langle p|H'|p\rangle) = 0$. Therefore, the off-diagonal term of the AB′ structure is always zero, in agreement with the above mirror-symmetry analysis.

The above analysis shows that the MST must be driven by a combination of the mirror symmetry breaking and the interaction, which effectively distinguishes the two originally equivalent sublattices (A and B). The two sublattices are always equivalent without the interaction. They remain equivalent with interaction if the mirror symmetry is preserved when squashing because the interaction occurs between atoms from two sublattices in a symmetric manner. Only if the mirror symmetry is broken when squashing and hence the interaction occurs between atoms within only one sublattice (A), will make it distinguishable from the other sublattice (B).

Figure 10 provides a clear evidence of such a distinction of the two sublattices by the local density of states (LDOS). The LDOS distributions of two atomic layers (along z-axis) are plotted in Figure 10. Each layer consists of two sublattices (A and B) of 16 atoms. The LDOS near the Fermi energy of an ideal SWCNT are homogeneously distributed over the two equivalent sublattices. In AA′ squashed SWCNT, the electrons tend to distribute around A sites below the Fermi energy, but around B sites above it, causing a discontinuity in the energy spectrum, as shown in Figure 10(a). In AB′ squashed SWCNT (Fig. 10(b)), the LDOS crosses the Fermi energy continuously. The tiny inhomogeneity of the LDOS is caused by the inhomogeneous curvature of the squashed SWCNT.

3.1.2. *A Unified Model of MST in Squashing SWCNTs*

Different from armchair SWCNTs, zigzag SWCNTs can be either metal or semiconductor, as mentioned earlier. Experimental measurements and theoretical simulations both show that a MST can be achieved more easily in metallic zigzag SWCNTs than armchair SWCNTs.[3, 26, 27] Theoretical studies[26, 27] showed that the mechanism to drive a MST in metallic zigzag SWCNTs is different from that in armchair SWCNT. MST in squashing metallic zigzag SWCNTs is mainly driven by the curvature effect,[26, 27] regardless both the mirror symmetry and interaction between the two flattened faces. We[29] re-examined the two different mechanisms which driving MST in armchair SWCNTs and zigzag SWCNTs and presented a unified explanation for the MST in SWCNTs based on a simple tight-binding model: to make the two original equivalent sublattices *physically* distinguishable. This mechanism can also drive MST in a graphene monolayer, but, incidentally, not in a graphene bilayer.

Figure 11 illustrates energy dispersion relation of a simple tight-binding model of a one-dimensional lattice system. It can be described by a simple cosine function

$$\varepsilon - \varepsilon_0 = 2\gamma_0 \cos(ka) \tag{7}$$

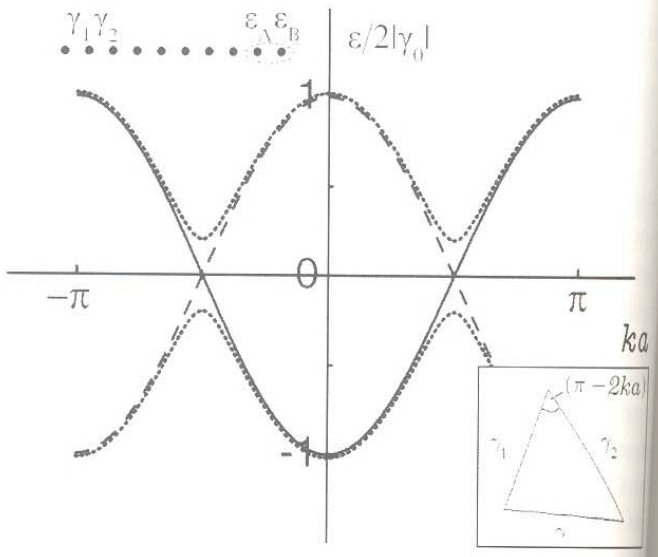

Fig. 11. The solid line: energy dispersion relation of one-dimensional latticed system; the dot line: energy dispersion relations of systems shown in the left-top corner. The right-bottom insert: the triangle relationship between γ and γ_1, γ_2. Reprinted with permission from [29], J. Q. Lu et al., *J. Appl. Phys.* 97, 114314 **(2005)**. © 2005, American Institute of Physics.

where, ε_0 is the onsite energy in the tight-binding model, γ_0 is the nearest-neighbor hopping integral, k is the one-dimensional wave vector, and a is the lattice constant. If the bands are half filled, the Fermi energy of the system is ε_0, and the curve of the energy dispersion relation continues at the Fermi energy, so the system is metallic.

If the one-dimensional system is divided into two sublattices with different onsite energies ε_A and ε_B, as in the left-top corner of Figure 11, the energy dispersion relation of the system will change to

$$\varepsilon - \varepsilon_0 = \pm\{\Delta^2 + (2\gamma_0 \cos(ka))^2\}^{1/2} \tag{8}$$

where, $\varepsilon_0 = (\varepsilon_A + \varepsilon_B)/2$, $\Delta = |\varepsilon_A - \varepsilon_B|/2$. The energy bands are plotted as the dotted line in Figure 11. An energy gap with value 2Δ is opened near the Fermi energy, indicating the system is semiconducting. Therefore, a difference in the onsite energies of the two sublattices leads to a MST in the one-dimensional tight-binding model.

Another mechanism leading to a MST in the one-dimensional system is: to make the nearest-neighbor hopping integral different. If the onsite energies are kept as ε_0, but the two nearest hopping integrals are changed to γ_1 and γ_2, as shown in the left-top corner of Figure 11, the energy dispersion relation of the system changes to:

$$\begin{aligned} \varepsilon - \varepsilon_0 &= \pm\gamma \\ \gamma &= (\gamma_1^2 + \gamma_1^2 + 2\gamma_1\gamma_2 \cos(2ka))^{1/2} \end{aligned} \tag{9}$$

where γ and γ_1, γ_2 can be treated as the three sides of a triangle, as shown in the right-bottom inset of Figure 11. To get $\gamma = 0$, the two conditions: $2ka = \pi$ and $\gamma_1 = \gamma_2$, must be satisfied. Therefore, γ will not be zero no matter the value of k, if the two hopping integrals γ_1 and γ_2 are different. Then energy bands will open an energy gap with value $2|\gamma_1 - \gamma_2|$ near the Fermi energy and the system will be semiconducting.

The above discussion illustrates two mechanisms that can drive a MST in the one-dimensional lattice system: (i) a difference in the onsite energies of the two sublattices and (ii) a difference in the nearest-neighbor hopping integrals. The effect of both mechanisms is to make the two original equivalent sublattices *physically* distinguishable.

The similar examination is applied to SWCNTs. It is found that only the first mechanism can lead to a MST in armchair SWCNTs, while either mechanism can drive a MST in metallic zigzag SWCNTs. A SWCNT is wrapped from a graphene sheet. The processes of wrapping a graphene sheet into a SWCNT and then squashing it will produce curvature. The effect of the curvature is shown in Figure 12(b). First, it will reduce the ppπ overlap between the nearest-neighbor carbon atoms to the original $\cos^2\alpha$; second, the σ orbital and π orbital between the nearest-neighbor carbon atoms will not be normalized. Both the two effects lead to different nearest-neighbor hopping integrals along the axis and the circumference.

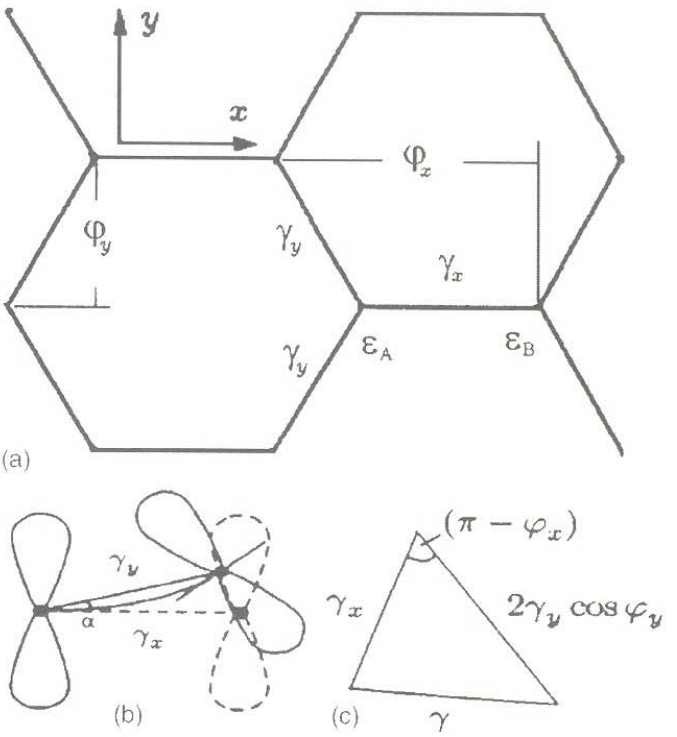

Fig. 12. (a) The graphene sheet-like structure with different onsite energies and nearest-neighbor hopping integrals. (b) The difference of γ_x and γ_y due to the curvature effect. (c) The triangle relationships between γ and γ_x and $2\gamma_y \cos\phi_y$. Reprinted with permission from [29], J. Q. Lu et al., *J. Appl. Phys.* 97, 114314 (**2005**). © 2005, American Institute of Physics.

On the other hand, squashing a SWCNT can also introduce new interactions between the atoms in one sublattice, as mentioned earlier. The new interaction distinguish the two sublattices from each other, which is equivalent to assigning different onsite energies to the two sublattices, as is the case in Boron-Nitride nanotubes. Therefore, with the process of wrapping and then squashing, the system shown in Figure 12(a) will be different from a graphene sheet, and it is assumed the two sublattices have different onsite energies ε_A and ε_B, and nearest-neighbor hopping integrals along the x and y directions given by γ_x and γ_y, respectively. The energy dispersion relation of such a system can be expressed as:

$$\varepsilon(k_x, k_y) - \varepsilon_0 = \pm(\Delta^2 + \gamma^2)^{1/2} \tag{10}$$

where, k_x and k_y are the wave vector components along the x and y directions, and

$$\begin{aligned} \varepsilon_0 &= (\varepsilon_A + \varepsilon_B)/2, \qquad \Delta = |\varepsilon_A - \varepsilon_B|/2 \\ \gamma &= (\gamma_x^2 + 4\gamma_y^2 \cos^2\varphi_y + 4\gamma_x\gamma_y \cos\varphi_x \cos\varphi_y)^{1/2} \end{aligned} \tag{11}$$

where φ_x and φ_y are half of the phase increments between the nearest-neighbor carbon atoms which belong to the same sublattice along the x and y directions, as shown in Figure 12(a), and $\varphi_x = \sqrt{3}k_x a/2$, $\varphi_y = k_y a/2$.

In order to keep the system metallic, there are two conditions must be satisfied: $\Delta = 0$, and $\gamma = 0$. Therefore,

a MST can be achieved by breaking of either condition. The different onsite energies from the two sublattices (i.e., $\Delta \neq 0$) leads to a MST. This mechanism can drive a MST not only in armchair SWCNTs, but also in all metallic SWCNTs and even in the graphene monolayer.

The other mechanism is to break the condition $\gamma = 0$. Figure 12(c) shows that γ can also be treated as one of the sides of a triangle, where the other two sides are γ_x and $2\gamma_y \cos\varphi_y$. That the condition $\gamma = 0$ can be further divided into two conditions: $\varphi_x = \pi$ and $2\gamma_y \cos\varphi_y = \gamma_x$. When a graphene sheet is wrapped into a SWCNT, $\varphi_x = \pi$ can be satisfied in both armchair SWCNTs and zigzag SWCNTs.

When a graphene sheet is wrapped in an armchair SWCNT and is squashed, the condition $2\gamma_y \cos\varphi_y = \gamma_x$ can always be satisfied. Though, the hopping integrals $\gamma_y \neq \gamma_x$ due to the wrapping and squashing, the φ_y can take any value near $\pi/3$ continuously because the restricted condition is applied on x direction. Thus, a difference in the nearest-neighbor hopping integral along the axis and the circumference will not drive a MST in armchair SWCNTs.

However, when a graphene sheet is wrapped into a zigzag SWCNT, the system is restricted in y direction. That φ_y can only take certain discrete values. Roughly, $\gamma_y = \gamma_x$ holds when a graphene sheet is wrapped into a SWCNT. The condition $2\gamma_y \cos\varphi_y = \gamma_x$ is $\cos\varphi_y = 1/2$, which means that φ_y can only be $\pm\pi/3$. This shows the well-known result that zigzag $(n,0)$ SWCNTs are metallic only when n is a multiple of 3. When squashing a metallic zigzag SWCNT, $\gamma_y \neq \gamma_x$, the condition $2\gamma_y \cos\varphi_y = \gamma_x$ can not be satisfied through adjusting φ_y, because φ_y can only take certain discrete values. Thus, a difference in the nearest-neighbor hopping integral along the axis and the circumference can be used to drive a MST in metallic zigzag SWCNTs.

In fact, it is impossible to maintain $\gamma_y = \gamma_x$ during the process in which a graphene sheet is wrapped into a SWCNT even without squashing. Thus, when n is a multiple of 3, there is a very narrow energy gap near the Fermi energy of zigzag $(n,0)$ SWCNTs, as shown in Figure 13(a).

Figure 13(a) shows the typical conductance curve of a perfect zigzag (12,0) SWCNT. As mentioned above, there is a very narrow gap near the Fermi energy. In Figure 13(b), when the SWCNT is squashed into an elliptical shape, a considerable gap is opened near the Fermi energy, indicating a MST. Further squashing the (12,0) SWCNT closes the conductance gap due to the enhanced $\sigma^* - \pi^*$ hybridization effects.[26]

A comparison of the MST in squashing zigzag (12,0) SWCNT and armchair (8,8) SWCNT is made in Figure 14. The variation of their conductance gaps are plotted as functions of the applied strain ε_{yy}. The strain ε_{yy} is defined by $\varepsilon_{yy} = (d - d_y)/d$. No MST in armchair (8,8) SWCNT takes place until it is squashed into a dumbbell shape that the opposite walls interact, which corresponds to $\varepsilon_{yy} = 0.76$ in Figure 14. However, a MST can be achieved more easily by squashing (12,0) zigzag SWCNT.

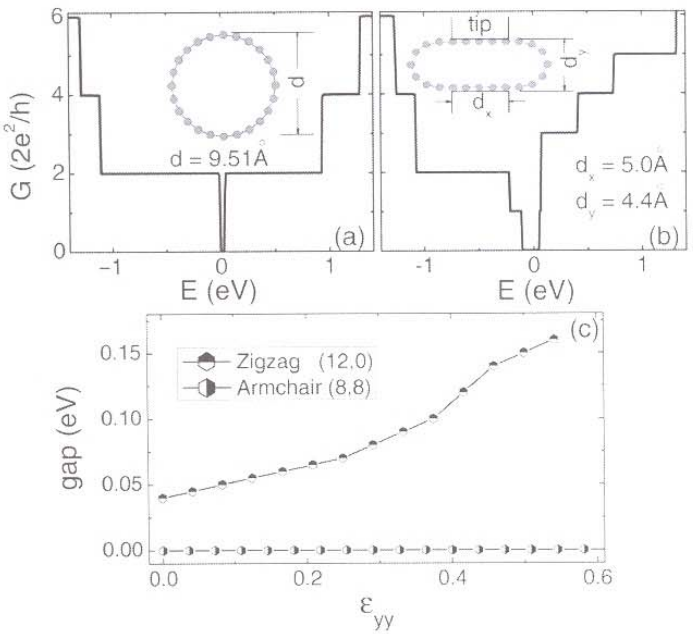

Fig. 13. (a, b) Conductances of different zigzag (12,0) SWCNT structures, as shown in the insets. E is the energy of conducting electrons. The Fermi energy of ideal zigzag (12,0) SWCNT is taken as zero. (c) The conductance gaps of zigzag (12,0) SWCNT and armchair (8,8) SWCNT as functions of the applied strain. Reprinted with permission from [29], J. Q. Lu et al., *J. Appl. Phys.* 97, 114314 (**2005**). © 2005, American Institute of Physics.

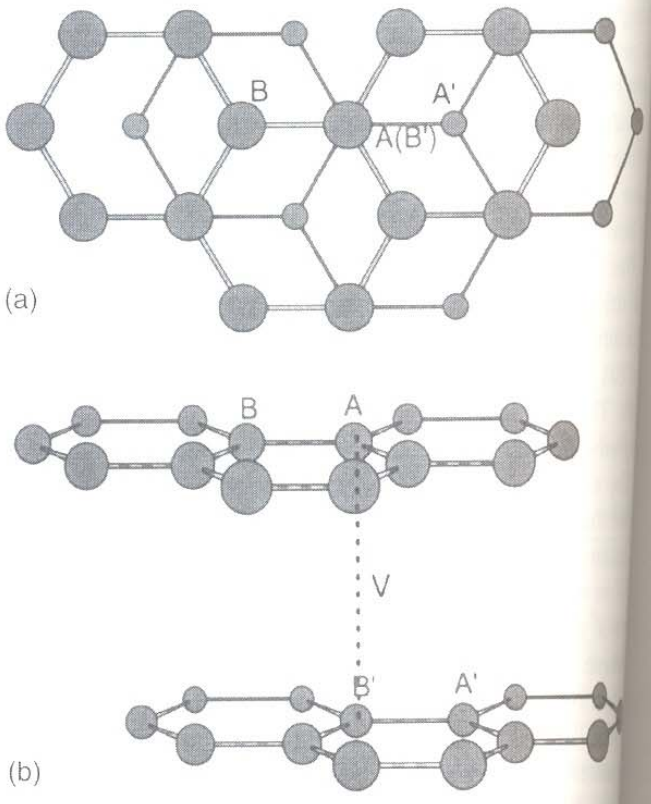

Fig. 14. The graphene bilayers with new interaction introduced between the sublattices A and B'. (a) Top view and (b) side view. Reprinted with permission from [29], J. Q. Lu et al., *J. Appl. Phys.* 97, 114314 (2005). © 2005, American Institute of Physics.

As mentioned earlier, the effect of the two different mechanisms which drive MST in one-dimensional tight-binding model is the same: to make the two original equivalent sublattices *physically* distinguishable. This is also true in the case of squashing SWCNTs.

Without squashing, the two sublattices in a graphene sheet or in a SWCNT are originally topologically distinguishable, but not *physically* distinguishable. The *physical* distinction means that the two sublattices are "felt" differently by the conducting electrons, which is the underlying reason for a MST. In the case of the first mechanism, the onsite energies of the two sublattices are different. That means the two sublattices are physically distinguishable.

In the case of the second mechanism, the nearest-neighbor hopping integral along the axis and the circumference are different, which also makes the two sublattices distinguishable. The condition $2\gamma_y \cos\varphi_y = \gamma_x$ in a graphene sheet can be understood to enforce the equality of the hopping integrals along the x direction (the axis direction of zigzag SWCNTs). In zigzag SWCNTs, when γ_x and γ_y is different, the equality is broken, which leads to the *physical* distinction of the two sublattices, as in the one-dimensional tight-binding model. In armchair SWCNTs, the axis direction is the y direction. The equality of the hopping integrals can always be satisfied. It is the reason that the second mechanism can not drive a MST in armchair SWCNTs.

Both the two different mechanisms which drive MST in squashing SWCNTs make the two original equivalent sublattices in SWCNTs *physically* distinguishable. The *physical* distinction between the two sublattices is a general mechanism which can drive a MST in any metallic SWCNTs or even in the graphene layers.

Though making the two sublattices *physically* distinguishable can drive a MST in a metallic SWCNT, it can not drive a MST in graphene bilayers. For example, a new interaction V is introduced between the sublattices A and B′ of the graphene bilayers, as shown in Figure 14. The two sublattices in each layer are physically distiguishable. The energy dispersion relation of the bilayer system can be expressed as:

$$\begin{aligned} \varepsilon - \varepsilon_0 &= (\mp V \pm \sqrt{V^2 + 4\gamma^2})/2 \\ \gamma^2 &= \gamma_0^2(1 + 4\cos^2\varphi_x + 4\cos\varphi_x \cos\varphi_y) \end{aligned} \tag{12}$$

where ε_0 is the onsite energy of the carbon atoms in the graphene bilayers and γ_0 is the nearest-neighbor hopping integral. $\varepsilon - \varepsilon_0 = \gamma$ is coincident the energy dispersion relation of a graphene monolayer, which can get the value 0 with given value of $\varphi_x = \pm\pi$ and $\varphi_y = \pm\pi/3$. At the same time, $\varepsilon - \varepsilon_0 = 0$ for the bilayer system, indicating that no energy gap is open and that no MST is achieved. This shows the difference between SWCNTs and graphene bilayers.

3.2. Finite Size Effect in Squashing SWCNTs and SWCNT-Based Structures and Devices Design

As mentioned above, MST may be achieved through squashing armchair SWCNTs. While theoretical studies[32] show that a local deformation usually can not drive a MST in armchair SWCNTs. The different conclusions are based on two different models: a radial deformation along the holistic SWCNT and a local deformation within only part of the SWCNT. The difference shows that the finiteness of the deformed length plays an important role in the electronic properties of SWCNTs. In case of SWCNT-based electronic device design, the deformed length along the SWCNT will be a key parameter to ensure their functions. We studied the finite size effect in a squashed armchair (10,10) SWCNT and proposed some SWCNT-based structures and devices design.

Figure 15(a) shows an example structure of an armchair (10,10) SWCNT squashed by a tip with finite length d_z = 6.0 Å. The cross section of the SWCNT changes from a dumbbell (in the fully deformed part of the SWCNT, as shown in Fig. 15(b)) to an ellipse (in the less deformed part, as shown in Fig. 15(c)), and then to a circle (in the undeformed part, as shown in Fig. 15(d)). In the fully deformed part, the smallest interatomic distance between the upper face and the lower face is $d_{AA'} = 2.1$Å, and the mirror symmetry is broken due to squashing. That the fully deformed part works as semiconductors.

Figure 16(a) shows the conductance curves near the Fermi energy of SWCNTs deformed by tips with different lengths. Though the fully deformed part acts as semiconductor, no energy gap is opened in the conductance curve if d_z is only 3.0 nm (the pink short dash line), that means the whole SWCNT keeps its metallic behavior.

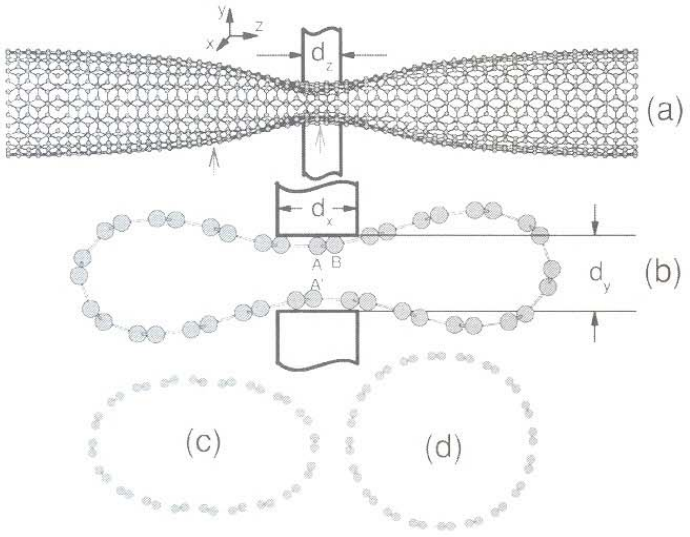

Fig. 15. (a) Finite length deformation in an armchair (10,10) SWCNT squashed by two identical tips; (b, c) cross sections of the different parts of the deformed SWCNT, as indicated by the arrows; (d) cross section of the non-deformed part of the SWCNT. Reprinted with permission from [25], J. Q. Lu et al., *Appl. Phys. Lett.* 84, 4203 (**2004**). © 2004, American Institute of Physics.

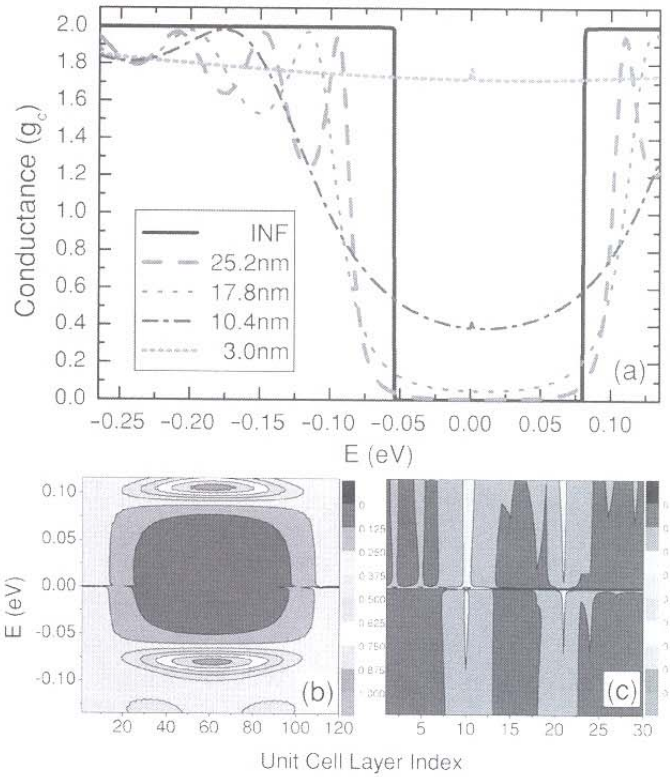

Fig. 16. (a) Conductance of armchair (10,10) SWCNTs deformed by tips with different length d_z. g_c ($= 2e^2/h$) is the unit quanta of conductance. E is the energy of conducting electron. The Fermi energy of ideal armchair (10,10) SWCNT is taken as zero. (b, c) The LDOS (unit: eV^{-1}) per unit cell layer near Fermi energy of SWCNTs deformed by tips with lengths (b) $d_z = 25.2$ nm and (c) $d_z = 3.0$ nm. Reprinted with permission from [25], J. Q. Lu et al., *Appl. Phys. Lett.* 84, 4203 (**2004**). © 2004, American Institute of Physics.

Moreover, the conductance of the whole SWCNT almost keeps constant near Fermi energy. When the tip length increases, the length of deformed part gets longer, the conductance near Fermi energy will begin to decrease, as shown in Figure 16(a). The conductance near Fermi energy approaches zero when $d_z = 25.2$ nm (the red dash line). When the tip length approaches infinite, the whole SWCNT is deformed, (which is the case of the radial deformation) the conductance near Fermi energy is zero.

Figures 16(b and c) present visual pictures of the finite size effect of deformation length in squashed SWCNTs. The LDOS per unit cell layer along the SWCNT axes are plotted. Each unit cell layer consists of 40 atoms which distribute over two atomic layers. When $d_z = 25.2$ nm, the deformed part of the squashed SWCNT contains about 100 unit cell layers (4000 atoms). The LDOS of layers in the deformed part and its nearby, totally 120 unit cell layers (4800 atoms), is plotted in Figure 16(b). The LDOS of the deformed part is almost zero near Fermi energy, which means that energy gap exists near Fermi energy within the deformed part. While in the nearby part, the LDOS crosses Fermi energy continuously. Consequently, the squashed SWCNT forms a metal-semiconductor-metal (MSM) heterojunction. It opens an easy way for SWCNT-based devices design. If $d_z = 3.0$ nm only, the deformed part only includes about 12 unit cell layers (480 atoms). The LDOS of 30 unit cell layers (1200 atoms) is plotted in Figure 16(c). Even in the deformed part, the LDOS crosses Fermi energy continuously. The SWCNT keeps its metallic behavior.

The underlying physics of the finite size effect of the deformed length in squashed armchair SWCNTs is the quantum tunnelling effect. When electron tunnels through an energy barrier, the tunnelling probability attenuate exponentially with increasing width of energy barrier. Electrons can easily tunnel through the energy barrier if it is narrow enough. This is particular important for nanoelectronic device design. If the size of the device is too small, electron can easily tunnel through the device, the device may not function well as expected.

Figure 17 gives a vivid sight of the tunnelling effect in the deformed SWCNT. The LDOS of each atom within one unit cell layer of the dumbbell part for the case $d_z =$ 25.2 nm and $d_z = 3$ nm are plotted in Figures 17(a and b). As mentioned earlier, when a MST is achieved in a squashed armchair SWCNT, the LDOS distributing on the two sublattices are distinguishable, which results in a discontinuity energy spectrum near Fermi energy. This phenomena can also be found in Figure 17(a), in the LDOS distribution of the dumbbell part of SWCNT deformed by tip with length $d_z = 25.2$ nm. Figure 17(b) shows the LDOS distribution of the dumbbell part of SWCNT deformed by tip with $d_z = 3.0$ nm. The distinction between the LDOS of the two sublattices is tiny. The LDOS crosses Fermi energy continuously. The LDOS near Fermi energy in the dumbbell part is resulted from the tunneling effect.

The interesting changes of the electronic structure in the SWCNT deformed by finite sized tip are also studied. Figure 17(c) shows the LDOS distribution within a unit cell layer of the ellipse part (as shown in Fig. 15(c)) of the SWCNT deformed by tips with $d_z = 25.2$ nm. It is interesting to find that the LDOS over the two sublattices are distinguishable, though there is no energy gap near Fermi energy with the absence of the bond formation between the flattened faces. Figure 17(d) plots the LDOS distribution within a circle unit cell layer, which is far from the deformed center with distance 40.6 nm. The LDOS of the two sublattices are also distinguishable. Moreover, the LDOS on one certain atom oscillates with energy, as indicated by the red dash line in Figure 17(d). Studies also show that the LDOS of the two sublattices within a unit cell layer are always distinguishable when the distance between the layer and the deformed center increases, and the oscillation of LDOS with energy becomes more exquisite. The LDOS of the ideal SWCNT near Fermi energy distribute over each carbon atom homogeneously. Upon deformation, the π and π^* wave functions in the SWCNT are mixed due to the breaking of the mirror symmetry. With the finite size

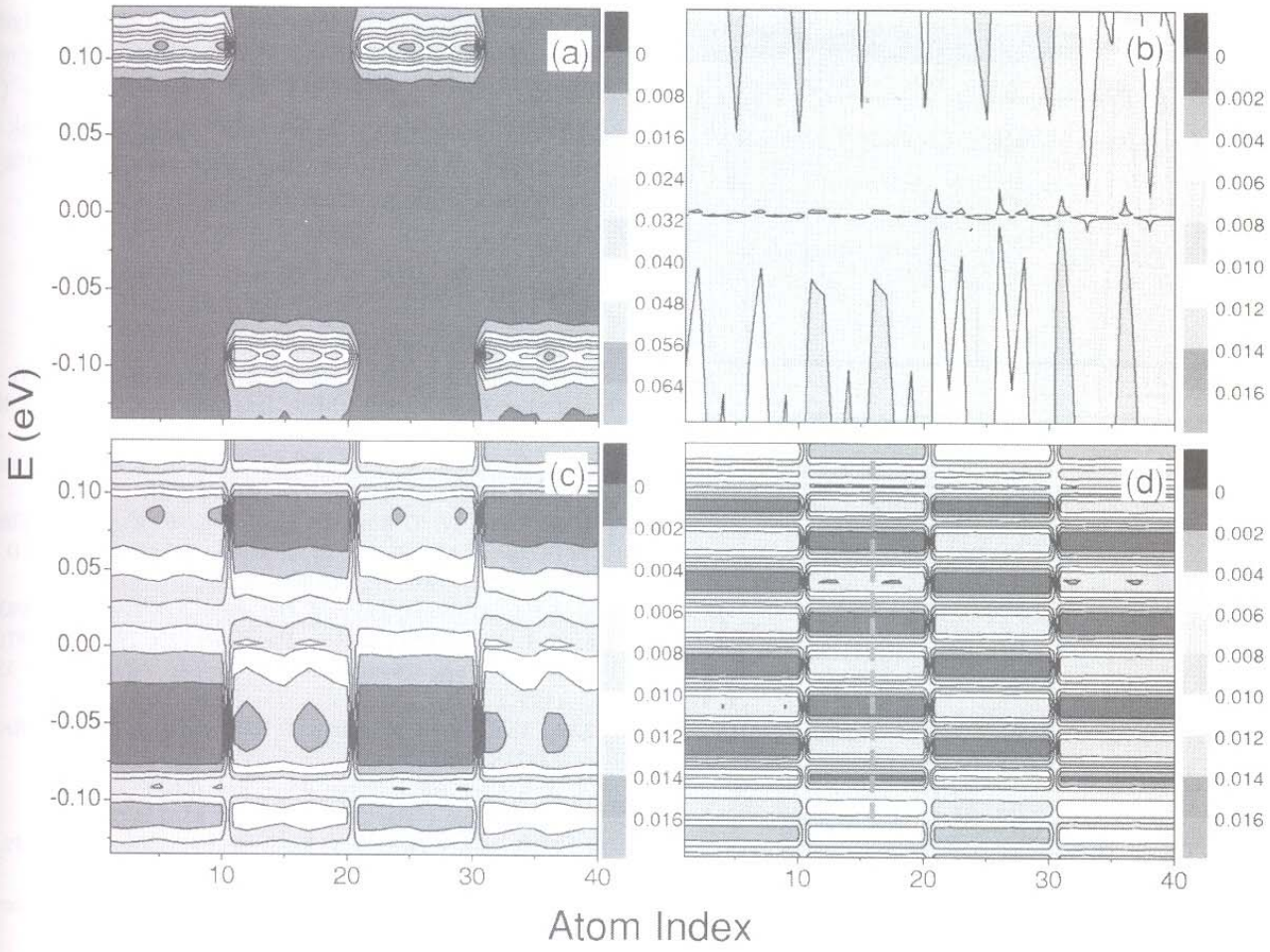

Fig. 17. The LDOS (unit: eV^{-1}) near Fermi energy within a unit cell layer of armchair (10,10) SWCNTs deformed by tips with different lengths (a, c, d) $d_z = 25.2$ nm and (b) $d_z = 3.0$ nm. (a, b) dumbbell part; (c) ellipse part and (d) circle part. The atoms in B (A) sublattice are labelled 1 (11) through 10 (20) for the first atomic layer and 21 (31) through 30 (40) for the second atomic layer. The dash line in (d) is added only for guide. Reprinted with permission from [25], J. Q. Lu et al., *Appl. Phys. Lett.* 84, 4203 (**2004**). © 2004, American Institute of Physics.

deformation, the translation symmetry along the SWCNT is also broken. The standing wave functions are the combination of the incoming and reflecting wave functions.[33] The LDOS near Fermi energy can be expressed as $2[1 \pm \cos(2\Delta kx)][1 + R \pm 2\sqrt{R}\cos(2k'_F x + \delta)]$.[34] The distinction between the LDOS of the two sublattices results from the difference between $[1 \pm \cos(2\Delta kx)]$. As the energy dispersion relations near Fermi energy is approximately linear with $\Delta k = 2E/(\sqrt{3}a\gamma_0)$, the period of the oscillation is $T_E = \sqrt{3}a\gamma_0\pi/(2x)$.

As mentioned above, an armchair (10,10) SWCNT can form a MSM heterojunction when the deformation length is large enough $d_z \sim 20$ nm. For the conducting electrons, the middle semiconductor layers act as an energy barrier. The MSM heterojunction opens up an easy way to structure some SWCNT-based nanoscale devices.

Figure 18(a) shows a SWCNT-based double barrier, by squashing an armchair SWCNT at two different positions. The typical behavior of double barrier structure is the resonant tunneling, as shown in the conductance curve in Figure 18(a). The small conductance peaks lying in the energy gap are due to the resonant tunnelling effect. The advantage of the SWCNT-based double barrier structure is that its electronic transport property can be easily controlled through changing the widths of the two energy barriers and the middle energy trap (i.e., changing the deformed length and the distance between the two deformed positions). For the example case shown in Figure 18(a), the tip length $d_z = 25.2$ nm, and the distance between the two deformed positions $l = 57.1$ nm.

If an armchair SWCNT is deformed periodically along its axis, it will behave as a superlattice, as shown schematically in Figure 18(b). The period of the superlattice in Figure 18(b) is $l = 57.1$ nm, and the tip length is $d_z = 25.2$ nm. The conductance of the nanoscale superlattice is also presented in Figure 18(b). As shown in the inset, each conductance peak is split into many small peaks. This is the resonant splitting effect of superlattice structure. The conductance vanishes near Fermi energy between the conductance bands. The electronic properties of the SWCNT-based superlattices can also be controlled easily through changing the range of the conductance gap. The latter can be achieved by adjusting the structure parameters.

For a logical circuit, transistor is one of the most important components. Designing a nanoscale transistor will be one of key steps to realize the nanologic. Bachtold et al.[35] achieved a nanoscale transistor experimentally. In their design, a semiconducting SWCNT is connected with two

REVIEW

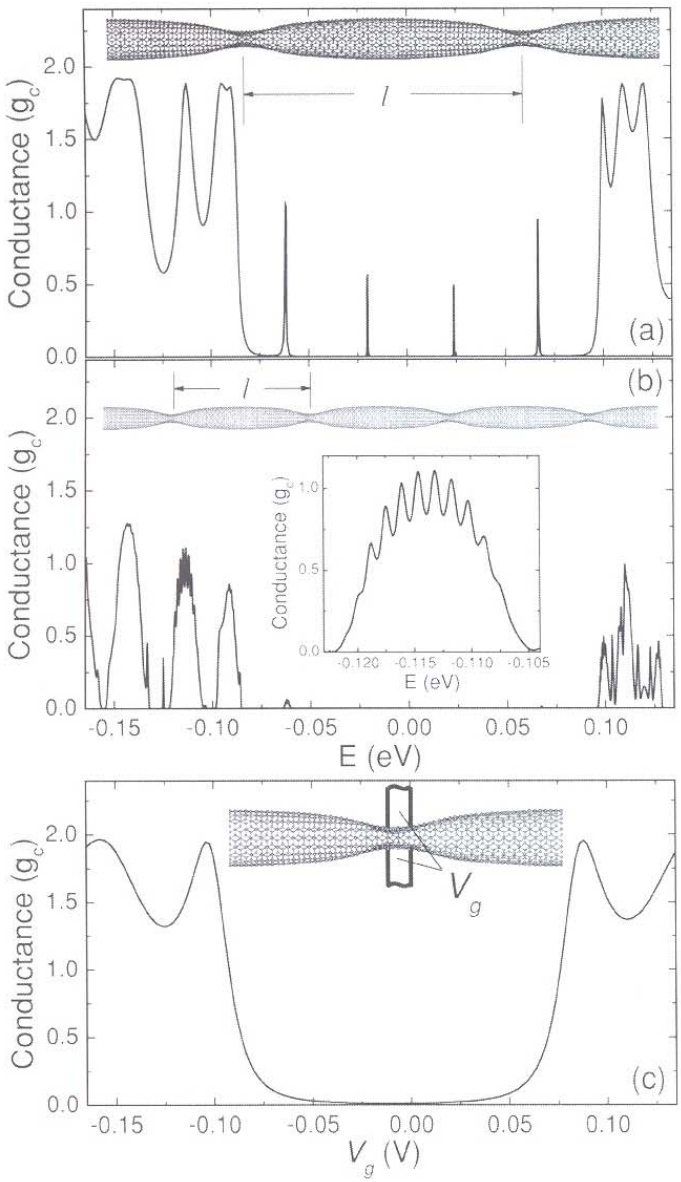

Fig. 18. Conceptual designs of SWCNT-based (a) double barrier; (b) superlattice; (c) transistor and their conductance curves. The structures are shown schematically only. The inset in (b) presents the detail of resonant splitting effect. Reprinted with permission from [25], J. Q. Lu et al., *Appl. Phys. Lett.* 84, 4203 (**2004**). © 2004, American Institute of Physics.

gold electrodes. Based on the MSM heterojunction, pure carbon transistor is possible.

Figure 18(c) shows of a conceptual design of pure carbon transistor based on MSM heterojunction with d_c = 25.2 nm. The MSM heterojunction will act as a nanoscale transistor if a gate voltage V_g is applied to the tips. When $V_g = 0$, as the deformed part behaves as semiconductor, the conductance is zero. The transistor is OFF. Changing of V_g will shift the energy gap of the deformed part. When Fermi energy does not lie in the shifted energy gap, the transistor begins to be ON. That is the basic principle of the SWCNT-based nanoscale transistor. Figure 18(c) also presents the dependence of the conductance on V_g. The logical voltage of the sample transistor is about −0.10 V.

Acknowledgment: Hanqing Jiang acknowledges the financial support from the Fulton School of Engineering at ASU. Part of this work was conducted at the Center for Nanophase Materials Sciences sponsored at Oak Ridge National Laboratory by the Division of Scientific User Facilities, US Department of Energy.

References

1. S. Iijima, *Nature* 354, 56 (**1991**).
2. T. W. Tombler, C. W. Zhou, L. Alexseyev, J. Kong, H. J. Dai, L. Lei, C. S. Jayanthi, M. J. Tang, and S. Y. Wu, *Nature* 405, 769 (**2000**).
3. E. D. Minot, Y. Yaish, V. Sazonova, J. Y. Park, M. Brink, and P. L. McEuen, *Phys. Rev. Lett.* 90, 4 (**2003**).
4. V. Semet, V. T. Binh, D. Guillot, K. B. K. Teo, M. Chhowalla, G. A. J. Amaratunga, W. I. Milne, P. Legagneux, and D. Pribat, *Appl. Phys. Lett.* 87, 3 (**2005**).
5. J. Cao, Q. Wang, and H. J. Dai, *Phys. Rev. Lett.* 90, 4 (**2003**).
6. C. L. Kane and E. J. Mele, *Phys. Rev. Lett.* 78, 1932 (**1997**).
7. R. Heyd, A. Charlier, and E. McRae, *Phys. Rev. B* 55, 6820 (**1997**).
8. L. Yang, M. P. Anantram, J. Han, and J. P. Lu, *Phys. Rev. B* 60, 13874 (**1999**).
9. A. Kleiner and S. Eggert, *Phys. Rev. B* 6307, 4 (**2001**).
10. L. Yang and J. Han, *Phys. Rev. Lett.* 85, 154 (**2000**).
11. C. Gomez-Navarro, J. J. Saenz, and J. Gomez-Herrero, *Phys. Rev. Lett.* 96, 076803 (**2006**).
12. C. Gomez-Navarro, P. J. de Pablo, and J. Gomez-Herrero, *Adv. Mater.* 16, 549 (**2004**).
13. T. Cohen-Karni, L. Segev, O. Srur-Lavi, S. R. Cohen, and E. Joselevich, *Nat. Nanotechnol.* 1, 36 (**2006**).
14. P. C. Collins, M. S. Arnold, and P. Avouris, *Science* 292, 706 (**2001**).
15. S. Rosenblatt, Y. Yaish, J. Park, J. Gore, V. Sazonova, and P. L. McEuen, *Nano Lett.* 2, 869 (**2002**).
16. P. Zhang, H. Jiang, Y. Huang, P. H. Geubelle, and K. C. Hwang, *J. Mech. Phys. Solids* 52, 977 (**2004**).
17. H. Jiang, P. Zhang, B. Liu, Y. Huang, P. H. Geubelle, H. Gao, and K. C. Hwang, *Comput. Mater. Sci.* 28, 429 (**2003**).
18. P. Zhang, Y. Huang, P. H. Geubelle, P. A. Klein, and K. C. Hwang, *Int. J. Solids Struct.* 39, 3893 (**2002**).
19. P. Zhang, Y. Huang, H. Gao, and K. C. Hwang, *J. Appl. Mech.-Trans. ASME* 69, 454 (**2002**).
20. D. W. Brenner, *Phys. Rev. B* 42, 9458 (**1990**).
21. M. Born and K. Huang, Dynamical Theory of the Crystal Lattice, Oxford University Press, Oxford (**1954**).
22. B. Liu, H. Jiang, H. T. Johnson, and Y. Huang, *J. Mech. Phys. Solids* 52, 1 (**2004**).
23. R. Saito, G. Dresselhaus, and M. S. Dresselhaus, Physical Properties of Carbon Nanotubes, Imperial College Press, London (**1998**).
24. C. H. Xu, C. Z. Wang, C. T. Chan, and K. M. Ho, *J. Phys.-Condens. Matter* 4, 6047 (**1992**).
25. J. Q. Lu, J. Wu, W. H. Duan, and B. L. Gu, *Appl. Phys. Lett.* 4203 (**2004**).
26. C. J. Park, Y. H. Kim, and K. J. Chang, *Phys. Rev. B* 60, 10 (**1999**).
27. P. E. Lammert, P. H. Zhang, and V. H. Crespi, *Phys. Rev. Lett.* 2453 (**2000**).
28. H. Mehrez, A. Svizhenko, M. P. Anantram, M. Elstner, T. Frauenheim, *Phys. Rev. B* 71, 7 (**2005**).
29. J. Q. Lu, J. Wu, W. H. Duan, B. L. Gu, and H. T. Johnson, *J. Phys.* 97, 4 (**2005**).

30. J. Q. Lu, J. Wu, W. H. Duan, F. Liu, B. F. Zhu, and B. L. Gu, *Phys. Rev. Lett.* 90, 4 (**2003**).
31. P. Delaney, H. J. Choi, J. Ihm, S. G. Louie, and M. L. Cohen, *Nature* 391, 466 (**1998**).
32. A. Maiti, J. Andzelm, A. Svizhenko, M. P. Anantram, and M. I. H. Panhuis, *Phys. Status Solidi B-Basic Res.* 233, 49 (**2002**).
33. J. Wu, W. H. Duan, B. L. Gu, J. Z. Yu, and Y. Kawazoe, *Appl. Phys. Lett.* 77, 2554 (**2000**).
34. H. F. Song, J. L. Zhu, and J. J. Xiong, *Phys. Rev. B* 66, 7 (**2002**).
35. A. Bachtold, P. Hadley, T. Nakanishi, and C. Dekker, *Science* 294, 1317 (**2001**).

Received: 18 April 2007. Accepted: 22 April 2007.

REVIEW